Surface brightness correction for compact extended sources observed by the *AKARI* Far-Infrared Surveyor in the slow-scan mode

Toshiya Ueta,[1] Rachael L. Tomasino,[1] Satoshi Takita,[2] Hideyuki Izumiura,[3,4] Mai Shirahata,[2] Andrew Fullard,[1] Issei Yamamura,[2] and Shuji Matsuura[2,5]

[1]*Department of Physics and Astronomy, University of Denver, Denver, CO 80208, USA*

[2]*Institute of Space and Astronautical Science, Japan Aerospace Exploration Agency, 3-1-1 Yoshinodai, Chuo, Sagamihara, Kanagawa 252-5210, Japan*

[3]*Okayama Astrophysical Observatory, National Astronomical Observatory of Japan, National Institutes of Natural Sciences, Honjo 3037-5, Kamogata, Asakuchi, Okayama 719-0232, Japan*

[4]*National Institutes of Natural Science, National Astronomical Observatory of Japan (NAOJ), Osawa 2-21-1, Mitaka, Tokyo 181-8588, Japan*

[5]*Kwansei Gakuin University, Department of Physics, School of Science and Technology, Gakuen 2-1, Sanda, Hyogo 669-1337, Japan*

ABSTRACT

We introduce a general-purpose surface brightness correction method for compact extended sources imaged in the slow-scan pointed-observation mode of the Far-Infrared Surveyor (FIS) aboard the *AKARI* infrared astronomical satellite. Our method recovers correct surface brightness maps by rescaling archived raw FIS maps using the surface-brightness-dependent inverse FIS response function. The flux of a target source is then automatically corrected for as the simple sum of surface brightnesses within the adopted target perimeter (i.e., standard contour photometry). This correction method is contrasted with the previous aperture photometry method for point sources, which directly corrects for the target flux with a flux-dependent scaling law. The new surface brightness correction method is applicable to objects of any shape from unresolved point sources to resolved extended objects, as long as the target is not deemed diffuse, i.e., the total extent of the target source does not exceed much more than a single FIS scan width of about $10'$. The new correction method takes advantage of the well-defined shape (i.e., the scale-invariance) of the point spread function, which enables us to adopt a power-law FIS response function. We analyze the point source photometric calibrator data using the FIS *AKARI* Slow-Scan Tool and constrain the parameters of the adopted power-law FIS response function. We conclude that the photometric accuracy of the new correction method is better than 10% error based on comparisons with the expected fluxes of the photometric calibrators, and that resulting fluxes without the present correction method can lead to differences more than a factor of two.

Keywords: infrared: general, methods: data analysis, methods: observational, techniques: image processing, techniques: photometric

1. INTRODUCTION

The Far-Infrared Surveyor (FIS: Kawada et al. 2007) is one of the two instruments on board the *AKARI* infrared astronomical satellite (*AKARI*; Murakami et al. 2007), covering from 50 to $180\,\mu$m with two sets of Ge:Ga arrays, the Short Wavelength (SW) and Long Wavelength (LW) detectors. *AKARI* swept the sky $3\rlap{.}'6\,\text{s}^{-1}$ during all-sky survey observations, covering more than 98% of the entire sky (the all-sky scan mode; Doi et al. 2015). During pointed observations, on the other hand, *AKARI* scan-mapped target objects at much slower $8\rlap{.}''0\,\text{s}^{-1}$ or $15\rlap{.}''0\,\text{s}^{-1}$ to achieve one to two orders of magnitude better sensitivity than the all-sky survey observations (the slow-scan mode; Shirahata et al. 2009).

The absolute surface brightness calibration of FIS was done through (1) pre-launch measurements of a blackbody source which indicated a 5% accuracy, and (2) in-orbit comparisons between FIS and COBE/DIRBE measurements of infrared cirrus regions without significant small-scale structures (Matsuura et al. 2011). However, when aperture photometry was performed for a set of infrared flux calibrators detected in the FIS slow-scan maps, the resulting fluxes were roughly 40% underestimates (Kawada et al. 2007; Shirahata et al. 2009). Such point-source flux underestimates were attributed to the response delay of Ge:Ga detectors to the incoming flux (known as "slow" transient responses) as previously reported by

Corresponding author: Toshiya Ueta
toshiya.ueta@du.edu

Coulais & Abergel (2000) for *ISO*/ISOCAM and Gordon et al. (2007) for *Spitzer*/MIPS. The slow transient response in scan observations of bright objects manifests itself as reduced surface brightnesses, resulting in lower source fluxes.

To address this issue, Shirahata et al. (2009) established a flux correction method for point sources detected in the FIS slow-scan maps. This method follows the point spread function (PSF) aperture correction technique and is based on the premise that the PSF shape is well-defined. However, this method would not work in general for objects that are neither point-like nor diffuse, because the surface brightness distribution of such objects is not known *a priori*. Hence, there is a clear need for a more versatile surface brightness correction strategy aimed at compact extended sources observed with the FIS slow-scan mode. Below, we briefly outline the newly-developed surface brightness correction method for FIS slow-scan maps, which is already described in detail elsewhere (Ueta et al. 2017).

2. THE SCALE-INVARIANCE OF THE PSFS AND THE POWER-LAW FIS RESPONSE FUNCTION

The PSF shape in FIS slow-scan maps was already determined to be stable irrespective of the source brightness and color (Shirahata et al. 2009; in particular, their Figures 3 and 4). Mathematically speaking, the observed PSF shape uniformity requires that the empirical FIS response function, R, is scale-invariant. Hence, because a power-law function is scale-invariant, we can assume a power-law function for R of the following form:

$$S_{ij,\mathrm{FIS}} = R(S_{ij,\mathrm{SKY}}) = c S_{ij,\mathrm{SKY}}^n, \tag{1}$$

where $S_{ij,\mathrm{SKY}}$ is the true surface brightness distribution of the observed sky (i and j referring to pixel positions), c and n are the power-law index and scaling coefficient of the response function, respectively, and $S_{ij,\mathrm{FIS}}$ is the surface brightness distribution seen in the resulting processed FIS maps. From equation (1), we can recover the true surface brightness distribution of the observed sky via

$$S_{ij,\mathrm{SKY}} = \left(\frac{S_{ij,\mathrm{FIS}}}{c} \right)^{\frac{1}{n}}, \tag{2}$$

and the true flux of a target object via

$$F_{\mathrm{OBJ}} = \sum_{ij} S_{ij,\mathrm{SKY}} = \sum_{ij} \left(\frac{S_{ij,\mathrm{FIS}}}{c} \right)^{\frac{1}{n}} = c^{-\frac{1}{n}} \sum_{ij} S_{ij,\mathrm{FIS}}^{\frac{1}{n}}, \tag{3}$$

where the summation symbol refers to the sum of pixels within the perimeter of the target object.

2.1. Super-PSFs

The *AKARI* slow-scan mapping data in the archive are stored in the time-series data (TSD) format. Therefore, TSDs need to be processed into co-added maps with some map-making software. We used the second-generation data reduction package, FIS *AKARI* Slow-scan Tool (FAST: Ikeda 2012), which allows more flexible and thorough corrections of TSD (e.g., a superior glitch and calibration lamp after-effect removal and more selective exclusion of data points that are affected by anomalies) than the first-generation pipeline software, FIS Slow-Scan data analysis Toolkit (SS-Tool: Matsuura et al. 2007) does. Another difference between FAST and SS-Tool is how photon energy is assumed to be distributed over the FIS arrays after each photon hit. SS-Tool always assumes a uniform distribution within the beam (i.e., a flat-top beam), whereas FAST can adopt user-selected profiles such as a Gaussian beam. The resulting FAST final co-added maps, which are supposedly flux-calibrated with respect to the diffuse cirrus emission, are made at the pixel scale of $8''$ pixel^{-1} (corresponding to roughly 1/4 to 1/6 of the nominal spatial resolution).

Hence, FAST-processed PSFs need to be checked for their scale-invariance before we proceed. To do so, we construct "super-PSF" maps in each of the four FIS bands by taking the median of the normalized and aligned FAST-processed images of the PSF/photometric references (of 24 and 18 sources for the SW and LW bands, respectively). Then, we compare individual PSF reference maps with the super-PSF map to compute the median of the absolute differences between each PSF image and the super-PSF image, i.e., the median absolute deviation (MAD) for each band (Figure 1). The MAD maps graphically represent how individual PSFs are statistically different from the super-PSF image at each pixel. Within the region that registers more than 5σ (the outer contour in Figure 1), the median MADs intrinsic to the source emission are $0.5 \pm 0.6\,\%$, $0.8 \pm 0.4\,\%$, $2.4 \pm 0.7\,\%$, and $4.1 \pm 2.1\,\%$, for the *N60*, *WIDE-S*, *WIDE-L*, and *N160* bands, respectively. These values indicate that the PSF shape in FIS maps is identical more than $99\,\%$ in the SW bands and more than $95\,\%$ in the LW bands. Therefore, the PSF shape is indeed uniform irrespective of the source brightnesses and object colors/temperatures, i.e., scale-invariant (at least within the scan speed, reset interval, and cross-scan shift length used to obtain the PSF reference data).

2.2. Parameters of the FIS Power-Law Response Function

The duly-warranted scale-invariance of the empirical FIS response function allows us to adopt a power-law function (Equation 1). Then, we need to determine the power-law index, n, and scaling coefficient of the response function, c. The
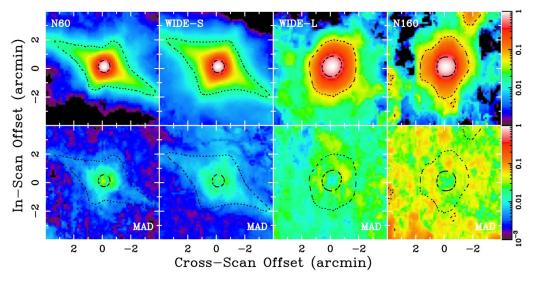
Figure 1. The *AKARI*/FIS super-PSF images (top row) and the corresponding median absolute deviation (MAD) maps (bottom row) in the *N60*, *WIDE-S*, *WIDE-L*, and *N160* bands (from left to right). The logarithmic color scaling of the images, from 0.1 % to 100 % relative to the peak intensity, is indicated in the wedge on the right. The dashed and dotted contours in the PSF surface brightness distribution images represent the FWHM and $5\,\sigma$ levels, respectively.

power-law exponent n is equivalent to the slope of the $\log(S_{ij,\mathrm{FIS}}) - \log(S_{ij,\mathrm{SKY}})$ plot. However, because we do not know $S_{ij,\mathrm{SKY}}$ *a priori*, we need a proxy for $S_{ij,\mathrm{SKY}}$. For the PSF/photometric references, we already know the expected model fluxes, $F_{\mathrm{PSF,model}} = \sum S_{ij,\mathrm{SKY}}^{\mathrm{PSF}}$. Hence, we can use $F_{\mathrm{PSF,model}}$ as a single-valued proxy for $S_{ij,\mathrm{SKY}}$ of PSF/photometric references. Then, we need a corresponding single-valued proxy for $S_{ij,\mathrm{FIS}}$. We adopt the observed peak intensity of the PSF, $I_{\mathrm{peak,FIS}}$, as a single-valued proxy for $S_{ij,\mathrm{FIS}}$, because $F_{\mathrm{PSF,observed}} = \sum S_{ij,\mathrm{FIS}}^{\mathrm{PSF}} = I_{\mathrm{peak,FIS}} \sum f_{ij}$, where f_{ij} is the normalized super-PSF profile. Therefore, we can constrain n as the slope of the $\log(I_{\mathrm{peak,FIS}}) - \log(F_{\mathrm{PSF,model}})$ plot.

Next, we need the scaling coefficient of the response function, c. Ideally, FIS maps would recover the true surface brightness distribution of the sky when the maps are properly rescaled by the inverse FIS response function (Equation. 2). Hence, rescaled FIS maps would yield the expected fluxes of the PSF references via contour photometry, i.e., $F_{\mathrm{PSF,model}} \geq F_{\mathrm{PSF,observed}} = \sum S_{ij,\mathrm{SKY}}^{\mathrm{PSF}} = \sum[(S_{ij,\mathrm{FIS}}^{\mathrm{PSF}}/c)^{1/n}] = c^{-1/n} \sum[(S_{ij,\mathrm{FIS}}^{\mathrm{PSF}})^{1/n}]$. The inequality symbol in the last equation refers to the fact that the measured PSF flux, as the sum of pixel values within a user-defined finite-sized photometric contour in a rescaled PSF surface brightness map, is always equal to or smaller than the expected/model PSF flux, $F_{\mathrm{PSF,model}}$, which can be recovered in the idealized infinite aperture. We can derive c by fitting the linear relation, $\sum_{3\sigma}[(S_{ij,\mathrm{FIS}}^{\mathrm{PSF}})^{1/n}] = c^{1/n} F_{\mathrm{PSF,3\sigma}}$. Here, $3\,\sigma$ indicates that the corresponding values are evaluated/scaled within the $3\,\sigma$ contour. The derived n and c values are listed in Table 1.

Table 1. Parameters and Characteristics of Flux Correction for Contour Photometry

Band	Power-Law Fit Parameters		Correction Accuracy	Flux Range
	n	c	[%]	[Jy]
N60	0.91±0.01	1.08±0.01	94 ± 10	0.14 – 320
WIDE-S	0.90±0.01	1.28±0.01	92 ± 9	0.10 – 360
WIDE-L	0.92±0.01	1.39±0.02	88 ± 7	0.41 – 270
N160	0.96±0.02	0.52±0.01	92 ± 20	1.7 – 250

NOTE—The derived (n, c) parameters are valid only when the surface brightness units of the input *AKARI* slow-scan maps are given in MJy sr^{-1}.

3. **RESULTS OF THE NEW SURFACE BRIGHTNESS CORRECTION METHOD**

Now that we have the power-law index, n, and scaling coefficient of the response function, c, determined, we can rescale FAST-processed FIS maps to recover the true surface brightness distribution of a target object and the neighboring sky background (Equation 2) and derive the true flux of a target object (Equation 3). To demonstrate the effectiveness of the correction method, we show how uncorrected and corrected fluxes (measured from uncorrected and corrected surface brightness maps, respectively) of PSF/photometric references compare with their expected/model fluxes. The left four
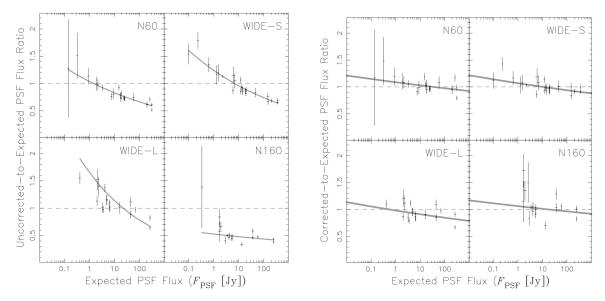
Figure 2. The uncorrected-to-expected (left) and corrected-to-expected (right) PSF flux ratios as a function of the expected PSF flux in each FIS band as indicated. These fluxes are measured by summing all surface brightness pixel counts within the 3σ aperture. The gray solid lines show the power-law best fits.

frames of Figure 2 are plots of the uncorrected-to-expected flux ratio as a function of the expected flux in each FIS band, exhibiting the rather strong brightness-dependent response of the FIS detector stemming from the slow-transient response. The brightness-dependent response can result in up to a factor of two difference. On the other hand, the right four frames of Figure 2 are plots of the corrected-to-expected flux ratio as a function of the expected flux in each FIS band, showing that the brightness-dependent response of the FIS detector is sufficiently suppressed by the present surface brightness correction method. The power-law best-fit for the corrected-to-expected PSF flux ratios are $(1.08 \pm 0.04) \times F_{\mathrm{Jy}}^{(-0.02 \pm 0.01)}$, $(1.07 \pm 0.02) \times F_{\mathrm{Jy}}^{(-0.03 \pm 0.01)}$, $(0.98 \pm 0.03) \times F_{\mathrm{Jy}}^{(-0.03 \pm 0.01)}$, and $(1.06 \pm 0.04) \times F_{\mathrm{Jy}}^{(-0.02 \pm 0.01)}$, for the *N60*, *WIDE-S*, *WIDE-L*, and *N160* bands, respectively, where F_{Jy} is the 3σ expected flux in Jy. These fits suggest that the flux uncertainty is roughly 10 %. The effective accuracy of the flux correction and the range of applicability are also included in Table 1.

4. SUMMARY

We have established a general method to recalibrate *AKARI*/FIS slow-scan surface brightness images based on the empirical power-law FIS response function suggested by the scale-invariance of the PSF shape in the FIS maps. The purpose of this method is to recover the correct surface brightness distribution of compact extended sources, which are more extended than point sources but less extended than diffuse background, and derive their fluxes as the simple sum of surface brightnesses within an appropriately-defined perimeter of the target sources. This method is applicable to any objects (including point sources) provided that the source is not considered diffuse (i.e., less extended than about 10′, which is the nominal single scan angular width). Those who wish to use *AKARI*/FIS slow-scan maps for science involving objects that are compactly extended (i.e., circumstellar shells, nebulae, nearby galaxies, etc) are encouraged to adopt this correction procedure to obtain correct surface brightness distributions of the target sources.

ACKNOWLEDGMENTS

REFERENCES

Coulais, A., & Abergel, A. 2000, A&AS, 141, 533
Doi, Y., Takita, S., Ootsubo, T., et al. 2015, PASJ, 67, 50
Gordon, K. D., Engelbracht, C. W., Fadda, D., et al. 2007, PASP, 119, 1019
Ikeda, N. 2012, FAST User's Handbook, ver. 0.1 (Sagamihara: ISAS)
Kawada, M., Baba, H., Barthel, P., et al. 2007, PASJ, 59, S389
Matsuura, S., Shirahata, M., Kawada, M., et al. 2007, PASJ, 59, S503
Matsuura, S., Shirahata, M., Kawada, M., et al. 2011, ApJ, 737, 2
Murakami, H., Baba, H., Barthel, P., et al. 2007, PASJ, 59, S369
Shirahata, M., Matsuura, S., Hasegawa, S., et al. 2009, PASJ, 61, 737
Ueta, T., Tomasino, R. L., Takita, S., et al. 2017, PASJ, 69, 11